Exploring the catalytic properties of supported palladium catalysts in the transfer hydrogenolysis of glycerol

F. Mauriello[1,*], H. Ariga[2], M.G. Musolino[1], R. Pietropaolo[1], S. Takakusagi[2], K. Asakura[2,*]

[1] *Dipartimento di DICEAM, Università Mediterranea di Reggio Calabria, Loc. Feo di Vito, I-89122 Reggio Calabria, Italy*

[2] *Catalysis Research Center, Hokkaido University, Kita-ku N21W10, Sapporo, Hokkaido 001-0021, Japan*

**Corresponding authors.*

Tel: +39 0965875278 - Fax: +39 0965875248
E-mail: francesco.mauriello@unirc.it (F. Mauriello)

Tel and Fax: +11 7069113
E-mail: askr@cat.hokudai.ac.jp (K. Asakura)

Keywords: Catalytic Transfer Hydrogenolysis (CTH), Glycerol valorization, 1,2-Propanediol, Coprecipitated palladium catalysts, Strong Metal Support Interaction.

Abstract

The transfer hydrogenolysis of glycerol promoted by supported palladium catalysts is reported. The reactions were carried out under mild conditions (453 K and 5 bar of N_2) in absence of added hydrogen by using the reaction solvent, 2-propanol, as hydrogen source. The catalytic results are interpreted in terms of metal (Pd) – metal (Co or Fe) interaction that modifies the electronic properties of palladium and affords bimetallic PdM sites (M = Co or Fe), thus enhancing the catalytic properties of the systems in the conversion of glycerol as well as in the selectivity to 1,2-propanediol and 1-propanol. The transfer hydrogenolysis mechanism is here elucidated and involves the glycerol dehydration to 1-hydroxyacetone and the subsequent hydrogenation of 1-hydroxyacetone to propylene glycol.

1. Introduction

The use of renewable biomass for bulk chemicals production provides a viable route for the modern chemical industry to alleviate its historical dependence on fossil resources and to reduce, at the same time, CO_2 emissions [1]. Among several catalytic processes for upgrading biomass derived compounds, "bio"-hydrogenolysis has gained a lot of attention bearing the potential to bridge available technologies and future refinery concepts [2]. Surely, one of the main targets is currently to make the hydrogenolysis a self-sustainable process and to reduce the costs related to hydrogen purchase, transport and storage and to minimize safety problems in industrial hydrogenation processes. Catalytic transfer hydrogenolysis (CTH) reactions [3] represent an interesting alternative to the direct use of molecular hydrogen. Together with traditional hydrogen donors (cyclohexane, hydrazine, formic acid and formates), simple alcohols can be used in CTH reactions with secondary alcohols generally more active than primary alcohols due to the higher electron-releasing inductive effect.

Glycerol is the major by-product in the industrial production of biodiesel and it is also a model molecule for biomass derived polyols keeping the potential to become a new primary building block [4]. Indeed, glycerol can be converted, through the hydrogenolysis reaction [5], into valuable products such as 1,2-propanediol (1,2-PDO), 1,3-propanediol (1,3-PDO) and ethylene glycol (EG), widely used in the synthesis of polyester fibers and resins, pharmaceuticals, cosmetics, flavours and fragrances, antifreeze, among others.

While several active metals and metal oxides supports [6] have been widely studied in the hydrogenolysis of glycerol, palladium has not been investigated significantly. In recent years, the coprecipitated palladium on iron oxide (Pd/Fe) catalyst, has been deeply tested showing superior performance in a number of reactions such as: aqueous-phase reforming of ethylene glycol [7], ethylene glycol dehydroxylation [8], aliphatic carbonyl reduction [9] and glycerol hydrogenolysis [10]. Furthermore, the same Pd/Fe catalyst can be used in the CTH of glycerol [11] and in the sequential transfer hydrogenation/hydrogenolysis of furfural and 5-hydroxymethylfurfural [12].

It is generally accepted that coprecipitated catalysts are characterized by an intimate interaction between the active metal and the oxide-support; however, mixture of single/mixed oxides phases and not uniform distribution of the active metal do also occur [13]. This complexity, by itself, does not allow to fully understand the role of the different components in coprecipitated catalysts. In this context, a comparison between the catalytic activity of palladium catalysts supported on iron oxide and cobalt oxide prepared both by coprecipitation and impregnation techniques should be widely welcome.

The present study aims to clarify the effect of individual parameters such as surface area, metal particle size, oxidation state of palladium, role of the support and presence of bimetallic clusters which may affect the catalytic properties of palladium catalysts in the transfer hydrogenolysis of glycerol. More fundamental understanding might, in fact, help a further and more rational optimization of the synthesis parameters in order to drive the catalytic properties of coprecipitated catalysts. Therefore, X-ray diffraction (XRD), transmission electron microscopy (TEM), CO chemisorption (S_{act}), temperature-programmed reduction by H_2 (H_2-TPR) and X-ray photoelectron spectroscopy (XPS) were performed to characterize structures and surface properties of palladium catalysts.

The catalytic conversion of glycerol to 1,2-propanediol, 1-propanol and ethylene glycol was carried out in absence of additional H_2 with the reaction solvent (2-propanol) being the source of the necessary hydrogen. The comparison of results involves, on one hand, coprecipitated Pd/Co and Pd/Fe catalysts and, on the other hand, impregnated Pd/Co_3O_4, Pd/CoO, Pd/Fe_2O_3 and Pd/Fe_3O_4 samples as well as a model catalyst such as commercial Pd/SiO_2. This broad set of Pd catalysts was chosen to get a wide framework of the factors that characterize the catalysts behaviour.

The relationship between the physico-chemical properties of palladium based catalysts and their catalytic performance is elucidated. The final aim is to draw up a deep insight on the key factors which make coprecipitated palladium systems very peculiar and unique in affording glycerol CTH. The correlation of the physico-chemical properties of the investigated Pd-based catalysts with the catalytic tests on glycerol CTH suggests that the catalyst preparation method plays a crucial role in determining

the electronic properties of palladium and in affording bimetallic PdM sites (M = Co or Fe) so that unusual catalytic properties can derive.

Furthermore, an insight on the ability of palladium catalysts to dehydrogenate 2-propanol, thus supplying the hydrogen necessary for the CTH reaction to occur, is included. A thorough examination of the reaction mechanism with hydroxyacetone (AC) being the key-intermediate is finally proposed.

2. Experimental Section

2.1 Catalysts preparation

All chemicals were purchased from Sigma-Aldrich and used without further purification. Supported palladium catalysts, with a nominal palladium loading of 5 wt %, were obtained by using two different techniques: coprecipitation and impregnation.

Pd/Co and Pd/Fe catalysts were prepared by using the coprecipitation technique and were obtained from aqueous solutions of the corresponding inorganic precursors. Anhydrous palladium chloride (Fluka, purum, 60 % palladium) was dissolved in HCl and cobalt(II) nitrate hexahydrate (Fluka, purity ≥ 99 %) or iron(III) nitrate nonahydrate (Fluka, purity ≥ 98 %) were added. The obtained aqueous metal salt solutions were added dropwise into a 1 M aqueous solution of Na_2CO_3. After filtration, samples were washed until complete removal of chloride ions, dried for 1 day at 353 K under vacuum and further reduced at 473 K for 2h under a flow of hydrogen.

Catalysts prepared by incipient wetness impregnation (Pd/Co_3O_4, Pd/CoO, Pd/Fe_3O_4 and Pd/Fe_2O_3) were obtained by adding a solution of palladium(II) acetylacetonate (Aldrich, purity 99 %) dissolved in acetone to commercially available supports Co_3O_4 (Aldrich, S_{BET}=40-70 $m^2\,g^{-1}$), CoO (Aldrich, S_{BET}=7 $m^2\,g^{-1}$), Fe_2O_3 (Sigma–Aldrich, S_{BET}=4 $m^2\,g^{-1}$) and Fe_3O_4 (Aldrich, S_{BET}=60 $m^2\,g^{-1}$). After impregnation, samples were dried for 1 day under vacuum at 353K and reduced at 473 K for 2h under a flow of hydrogen.

In order to determine the exact amount of Pd on our supports an X-ray fluorescence (XRF) analysis was carried out and the results are reported in Table 1.

Table 1 about here

2.2 Catalysts Characterization

XRD data were acquired at room temperature on a Philips X-Pert diffractometer by using the Ni β-filtered CuKα radiation (λ=0.15418 nm). Analyses were performed on samples reduced at 473 K for 2h

and registered in the 2θ range of 10–80° at a scan speed of 0.5°min^{-1}. Diffraction peaks were compared with those of standard compounds reported in the JPCDS Data File.

The particle size and the relative morphology of investigated catalysts were analysed by performing Transmission Electron Miscroscopy (TEM) measurements using a JEM-2100F (JEOL, Japan) operating at an acceleration voltage of 200 kV and directly interfaced with a computer controlled-CCD for real-time image processing. The specimens were prepared by grinding the reduced catalyst powder in an agate mortar and then suspending it in 2-propanol. A drop of the suspension, previously dispersed in an ultrasonic bath for 1 hour, was deposited on a copper grid coated by a holey carbon film. After evaporation of the solvent, the specimens were introduced into the microscope column. Particle size distributions were obtained by counting several hundred particles visible on the micrographs on each sample. From the size distribution, the average diameter was calculated by using the expression: $d_n = \Sigma n_i d_i / n_i$ where n_i is the number of particles of diameter d_i.

H_2-TPR measurements were performed using a conventional TPR apparatus. The dried samples (50mg) were heated at a linear rate of 10 K min^{-1} from 233 to 1273 K in a 5vol % of H_2/Ar mixture at a flow rate of 20 cm^3 min^{-1}. The H_2 consumption was monitored with a thermal conductivity detector (TCD). A molecular sieve cold trap (maintained at 193 K) and a tube filled with KOH, placed before the TCD, were used to block water and CO_2, respectively. The calibration of signals was done by injecting a known amount of H_2 into the carrier.

The active surface areas (S_{act}) were determined by CO-pulse chemisorption technique using a Micromeritics ChemiSorb 2750 system at room temperature. Samples were first reduced with H_2 at 25 stp ml/min usign a 10 K/min ramp up to 473 K, then cleaned with He at 25 stp ml/min for 15 min and finally cooled to room temperature. CO pulses (0.64 stp mL, 5% CO/He – 1,29 μmol CO each injection) were injected until saturation. S_{act} values were calculated by assuming a CO/Pd stoichiometry of 1 and a surface area of 7.87 x 10^{-20} m^2 per Pd atom [7].

XPS measurements were performed on a JPS-9010MC photoelectron spectrometer using an Al Kα (1486.6 eV) radiation source. After the reduction treatment, samples (denoted as "reduced") were introduced into the XPS chamber, avoiding exposure to air. In order to obtain the XPS spectra, the pressure in the analysis chamber was maintained at $5x10^{-9}$ mbar. All spectra were recorded at room temperature, and the binding energies (BE) were set taking the C 1s peak at 284.6 eV as reference. XPS spectra of reduced catalyst samples were also recorded after an additional "in situ reduction" condition (denoted as "in situ-reduced") in an auxiliary reaction chamber at 473 K under 100 Pa H_2 for 4 h.

Peak deconvolution and fitting analyses were performed using the peak-fitting software "SPECSURF, JEOL" including the spin-orbit splitting and relative intensities of the spin-orbit components fixed.

2.3 Catalytic Tests.

Hydrogenolysis reactions were performed in a 250 mL stainless steel autoclave at a stirring speed of 500 rpm. The reactor was first purged with N_2 (99.99%), the system was then pressurized with nitrogen and, finally, heated up to the reaction temperature. The temperature was monitored using a thermocouple inserted into the autoclave and connected to the thermocontroller. The standard reaction was carried out at 453 K and under 0.5 MPa initial N_2 pressure using a mixture of 75 mL 4 wt % glycerol in 2-propanol solution and 500 mg of the Pd-based catalyst previously reduced under H_2. After 24 hours of reaction, the system was cooled and the pressure was released carefully at room temperature.

The analysis of reaction products was performed with a gas chromatograph (Agilent 6890 GC) equipped with a wide bore capillarity column (CP-WAX 52CB, 50 m, inner diameter 0.53 mm) and a flame ionization detector. The conversion and selectivity of glycerol were calculated on the basis of the following equations:

$$conversion(\%) = \frac{moles\ of\ reacted\ glycerol}{moles\ of\ glycerol\ feed} \times 100$$

$$selectivity\ (\%) = \frac{moles\ of\ defined\ product}{moles\ of\ reacted\ glycerol} \times 100$$

3. Results

3.1 XRD analysis

XRD spectra of all investigated catalysts - after the reduction with H_2 at 473 K – are reported in Fig. 1.

Fig. 1 about here

In impregnated systems, the diffraction peaks belonging to the corresponding support structures, as well as to metallic Pd species (2θ = 40.01º), can be easily detected [14].

XRD patterns of coprecipitated catalysts reveal diffraction patterns related to Co_3O_4 and Fe_3O_4 [14]. The X-ray powder diffraction (XRD) pattern of the reduced Pd/Co catalyst shows strong and sharp diffraction peaks at 2θ values of 31.35, 36.98, 44.93, 59.52 and 65.36° corresponding to (220), (311), (400), (511), and (440) of pure cubic crystalline Co_3O_4. In addition, the presence of small diffraction peaks ascribed to pure cubic crystalline cobalt monoxide (diffraction peaks at 2θ values of 42.52, 61.54 and 77.52°) and hexagonal metallic cobalt (diffraction peak at the 2θ value of 47,09º) can be also observed. Moreovere, the presence of broad (111), (200), and (220) peaks, slightly shifted toward higher angles from those reported for pure Pd, are definitely indicative of the formation of a Pd-Co alloy [15].

On the other hand, the Pd/Fe sample pattern shows only peaks relative to Fe_3O_4. The absence of the (111) diffraction line of metallic palladium in the Pd/Fe sample is indicative of extremely small highly dispersed Pd-particles [16].

3.2 TEM analysis

Catalysts were also characterized by using TEM, that allows us to calculate the average size (Table 1) and the relative size distribution of palladium particles on the basis of size measurements of, at least, 100 particles for each sample. TEM images of coprecipitated and impegnated Pd catalysts at 50 and 5 nm and relative particles size distribution are reported in Fig. 2 and Fig. 3.

It appears also that, for impregnated catalysts reduced at 473 K, a broad distribution of palladium particles sizes is obtained. Although most of the particle diameters are in a range between 2 and 9 nm, a small quantity of larger particles is also observed.

Conversely, the Pd/Co catalyst shows the presence of faceted metal particles and is characterized by a broader size distribution, with a mean diameter of 10.7 nm, higher than that of other samples.

On the contrary, Pd/Fe exhibits a predominance of very small metallic particles and a relatively narrow particles sizes distribution with diameter values ranging between 0.5 and 2.5 nm, with the 1.2 nm dimension being the most commonly measured size.

Fig. 2 about here

Fig. 3 about here

3.3 H_2-TPR profiles

Fig. 4 shows H_2-TPR profiles of all investigated catalysts.

Fig. 4 about here

In Pd/Co_3O_4, Pd/CoO and Pd/Fe_2O_3 impregnated catalysts two peaks can be detected: the first at about 400 K belonging to the $Pd^{2+} \rightarrow Pd^0$ reduction (close to that of palladium acetylacetonate [17] used as precursor in the catalysts preparation), whereas the higher temperature peak at 645, 695 and 585 K, respectively, is assigned to the support reduction (slightly shifted towards lower temperatures with respect to the peak of the corresponding pure oxides [18, 19]).

Three characteristic H_2 consumption peaks appear in the Pd/Fe_3O_4 sample. While the peak centered at about 940 K can be easily related to the support reduction, the other two peaks at 373 and 433 K may be attributed to the reduction of differently dispersed Pd^{2+} containing species [20].

Hence, the TPR analyses of impregnated catalysts clearly indicate that poor interaction occurs between palladium and the supports.

On the other hand, H_2-TPR profiles of coprecipitated catalysts are characterized by only one broad and intense peak that can be related to the simultaneous reduction of palladium with cobalt-oxide or iron-oxide supports.

The profile of Pd/Co shows a broad and intense peak centered at about 535 K. This peak can be related to the simultaneous reduction of both palladium and cobalt cations causing shifts upward to that of palladium (PdO can be easily reduced by H_2 at room temperature) and downward to that of cobalt oxides (739 K) suggesting that Pd^{2+} containing species are stabilized within the cobalt-oxide support. This phenomenon is well documented in the literature and is attributed to the strong interaction between well dispersed Pd^{2+} ions and the metal oxide support [21]. Also the Pd/Fe H_2-TPR profile is characterized by a reaction area centered at about 360 K that includes, as confirmed by our H_2 consumption calculations, both $Pd^{2+} \rightarrow Pd^0$ and $Fe^{3+} \rightarrow Fe_3O_4$ reductions. The large shift of the reduction temperature relative to the reaction $Fe^{3+} \rightarrow Fe_3O_4$ from 694 K to 352 K is therefore ascribed to palladium particles which promote the reduction of Fe^{3+} to the Fe_3O_4 structure. Comparable results relative to coprepitated Pd/Fe catalysts, prepared by the same synthetic procedure, have been reported by other authors [7, 8, 12, 22] which draw analogous conclusions: Pd nanoparticles are effective in promoting the reduction of support from hematite to magnetite.

The most likely interpretation of the observed decrement in the reduction temperature of the oxide supports in Pd/Co and Pd/Fe systems can be related to palladium nanoparticles, highly dispersed inside the catalyst structure, which can easily produce spillover of hydrogen onto the Co or Fe oxide surfaces.

Thus, H_2-TPR measurements suggest that in Pd/Co and Pd/Fe coprecipitated samples intimate interactions of palladium cations with metal oxides supports are present.

3.4 XPS analysis

3.4.1 XPS analysis of the metal oxide supports

Fig. 5 about here

Table 2 about here

Table 3 about here

Fig. 5 shows the XPS spectra of "unreduced", "reduced" and "*in situ* reduced" samples. All the peaks were analysed by curve-fitting and the results are summarized in Tables 2 and 3.

The XPS spectra of unreduced, reduced and in situ-reduced impregnated samples evidence no shifts in binding energies values of Co $2p_{3/2}$ or Fe $2p_{3/2}$ (Tables 2 and 3) [23]. This result, in agreement with H_2-TPR analysis, shows that there is no modification of the support upon H_2 reduction at temperatures lower than 500 K.

On the other hand, coprecipitated samples show a different behavior. Fig. 5 evidences the $Co2p_{3/2}$ peak relative to Pd/Co samples. Unreduced and reduced Pd/Co catalysts (Fig. 5(a) and Table 2) show a broad peak at 780 eV, that corresponds to the coexistence of Co^{II} and Co^{III}. The satellite peak at 785.9 eV confirms the existence of cobalt(II)-oxide. After the in situ-reduction at 473 K, the satellite peak at 785.9 eV disappears and the $2p_{3/2}$ peak is shifted to a lower binding energy (778.0 eV), corresponding to that of metallic cobalt [18]. This point is very interesting since the reduction of $Co_3O_4 \rightarrow CoO$ in H_2 atmosphere proceeds at approximately 473K while the formation of metallic Co occurs only at higher temperature (up to 700K) [24]. In our case, the catalyst reduction occurs at 473K suggesting that the

presence of palladium facilitates the support reduction. It is worth to underline that XPS analysis on the Pd/Co catalyst is carried out also under "in-situ" reduction condition that allows to reveal the metallic cobalt. This latter cannot be easily observed through other characterization techniques (eg. XRD) because of the high tendency of cobalt to be oxidized in air.

In the case of Pd/Fe (Fig. 5 and Table 3), the presence of the satellite peak at about 718.8 eV on the unreduced catalyst indicates the Fe_2O_3 composition [23] whereas its absence on both "reduced" and "in situ reduced" samples suggests the Fe_3O_4 structure.

3.4.2 XPS analysis of palladium species

Tables 2 and 3 summarize the binding energies of the Pd $3d_{5/2}$ area for all samples. In all unreduced impregnated samples the Pd $3d_{5/2}$ peak appears at about 336.5 eV indicating the presence of totally oxidized Pd^{2+} species.

Upon H_2 treatment, the Pd $3d_{5/2}$ peak is shifted to lower binding energy values indicating the presence of metallic Pd [23].

In the reduced Pd/Co and Pd/Fe catalysts the binding energy of the Pd $3d_{5/2}$ level appears at about 0.5 eV value higher than that of the binding energy of metallic Pd (Fig. 6), indicating the presence of partial positively charged metal species ($Pd^{\delta+}$). Slightly higher binding energy values for the Pd $3d_{5/2}$ core level have been reported for bimetallic supported Pd catalysts [24] and assigned to alloy formation. Tsang and co-workers claimed [8] that the progressive shift to higher binding energy values in the Pd $3d_{5/2}$ area could be related to the increasing amount of 'Pd/Fe' clusters on the catalyst surface. Thus we could conclude that Pd-Co or Pd-Fe alloy nanoparticles might be present in the reduced coprecipitated catalysts.

Fig. 6 about here

3.5 Catalytic tests

Glycerol CTH data, relative to the reactions carried out in 2-propanol are listed in Table 4.

Table 4 about here

The best conversion was achieved with coprecipitated samples which are more active in glycerol C-O bond breaking but less efficient in C-C bond cleavage (small amounts of EG are formed). When using Pd/Co, the conversion of glycerol to 1-propanol (1-PO) is also observed.

Commercial Pd/SiO_2 and Pd/CoO catalysts show negligible activity in glycerol CTH and hydroxyacetone (AC) is the only reaction product observed. The other investigated samples (Pd/Fe_3O_4, Pd/Fe_2O_3 and Pd/Co_3O_4) are generally much less active than coprecipitated catalysts with the selectivity following the order AC ≥ 1,2-PDO > EG. Therefore, catalytic tests clearly indicate that coprecipitated Pd/Co and Pd/Fe catalysts are, by far, more efficient and selective towards 1,2-PDO than analogous impregnated samples.

The hydrogen necessary for the hydrogenolysis reaction derives from the dehydrogenation of the solvent (2-propanol). In order to confirm the solvent oxidation, analogous catalytic tests (500 mg of catalysts, 453 K for 24 h) were carried out on pure 2-propanol under inert atmosphere: only acetone, besides very small quantities of other products, is formed and its amount changes in the order Pd/Co > Pd/Fe > Pd/Fe_3O_4 > Pd/Fe_2O_3 ≅ Pd/Co_3O_4 > Pd/CoO. Interestingly, a tight relationship between the glycerol conversion and the amount of acetone formed during the CTH reactions is found (Fig. 7).

Fig. 7 about here

4. Discussion

4.1 Correlation of catalyst structural properties with the catalytic performance

Factors effecting the catalytic performance are usually discussed in terms of: (i) overall surface area, (ii) metal particle size, (iii) oxidation state of the metal centre, (iv) nature of the support (unreducible/reducible, acid/base sites) and (v) metal-metal and/or metal-support interactions. An accurate insight into all these parameters allows to discriminate which one is the most important factor in glycerol CTH.

Cross-check experiments, under the identical conditions used in this study, show that pure Co_3O_4, CoO, Fe_3O_4 and Fe_2O_3 do not give noticeable glycerol conversion in absence of palladium particles, suggesting that metal sites are an essential prerequisite for glycerol hydrogenolysis.

At the same time, the higher catalytic performance of coprecipitated catalysts with respect to analogous impregnated samples cannot be attributed to surface area or particle size effects: Pd/SiO_2 [25], with a specific surface area of 500 m^2/g was found to be nearly unactive towards glycerol hydrogenolysis. Furthermore, a direct correlation between the active-metal surface area and the catalytic activity and selectivity cannot be established. Therefore the first conclusion is that single palladium sites are generally to be considered poorly active in glycerol CTH reactions. Rather, we need to look at the interaction between the metal and the support structure in order to find the right way for understanding the large gap between the coprecipitated and the other Pd catalysts in the observed reactivity. In this regard, we recall that TPR, XRD and XPS analyses clearly show that the metal-oxide support is easily reducible in coprecipitated Pd/Co and Pd/Fe catalysts. In the case of the Pd/Co sample, when activated at 473 K with H_2, the support presents mainly the Co_3O_4 structure coupled with CoO and Co particles. Upon reduction, the conversion of Fe_2O_3 into Fe_3O_4 is also observed in the Pd/Fe catalyst. In both cases, the reduction process is catalyzed by palladium particles as demonstrated by H_2-TPR experiments.

However, the most important feature that allows to differentiate properties of coprecipitated catalysts from those of impregnated samples stays on the higher binding energy value of the $Pd3d_{5/2}$ core level (Tables 2 and 3) observed for Pd/Co and Pd/Fe substrates. These results indicate the possible formation of Pd-Co and Pd-Fe clusters that ensures electron modification on palladium particles affording an

easier glycerol conversion. In accord with our results, it was recently reported that the addition of Re to a Pd catalyst leads to formation of Re-Pd bimetallic particles which shows an increased conversion of glycerol and a higher selectivity to propanediols compared with the that of mono-component Pd catalysts [26]. At the same time, Co-Zn-Al [27] and RuFe/CNT [28] catalysts, were found to be highly active and stable towards the hydrogenolysis of polyols suggesting that the addition of Co and Fe as co-metals can increase the activity of Pd catalysts in glycerol CTH.

Even considering the complexity of coprecipitated catalysts structures, the preferential model deriving from our experimental results suggests that the co-precipitation technique, used for the preparation of Pd/Co and Pd/Fe catalysts, allows the deposition of Pd^{2+} ions or PdO nanoparticles embedded inside the support structure that increases the interaction between Pd cations and cobal/iron oxides and facilitates the formation of Pd-Co and Pd-Fe alloys after reduction.

As evidenced by XPS analysis, reduced coprecipitated catalysts are characterized by palladium particles with different electronic properties than those of impregnated samples and pure Pd. This electronic perturbation may lead to a better interaction of palladium (positively charged) with the OH group of glycerol, weakening the C–O bond and thus favoring hydroxyacetone formation. The presence of the positively charged palladium may be a crucial step in the overall reaction and derives from Pd-Co and Pd-Fe bimetallic interaction in coprecipitated catalysts.

An additional interesting point stems from the close correlation between glycerol conversion and acetone production from 2-propanol. Thus, the good performance of coprecipitated catalysts has to be attributed to two main factors: (i) the high ability to dehydrogenate 2-propanol into acetone and (ii) the high capability in C-O bond breaking.

In summary it should be definitely settled that, in CTH, the key factor raising the activity of coprecipitated catalysts is the strong interaction of palladium cations with the support leading, by reduction, to formation of bimetallic ensembles. Other factors such as surface area, metal particle size and nature of the support, are definitely less important.

4.2 Transfer hydrogenolysis (CTH) mechanism of glycerol by using 2-propanol as hydrogen source

Although several mechanisms have been suggested for glycerol hydrogenolysis, only few contributions are present in literature for CTH reactions [3c].

The proposed reaction mechanism (Scheme 1) has to take into account: (i) the formation of Pd-Co and Pd-Fe sites, (ii) the presence - in every experiment - of AC, (iii) the dehydrogenation of 2-propanol and (iv) a relative low hydrogen concentration in CTH reactions.

The first step is glycerol chemisorption on the catalyst surface. Computational studies [29] have established that in the case of glycerol, among several possible conformers, the most preferred is the one having two adjacent OH groups bound to metal sites. In our case, it may occur through a strong adsorption of two adjacent alcoholic groups of glycerol on Pd and Co(Fe) bimetallic site. The ensuing C-OH breaking, promoted by the alloyed palladium, is then followed by internal rearrangement of the unstable enol intermediate leading to AC. The substitution of hydroxylic group by hydrogen in organic alcohols occurs through SN_1 and SN_2 mechanisms, as reported for the hydrogenolysis of benzyl alcohol derivatives promoted by palladium systems [30]. In our case, the SN_2 path is quite unlikely since the hydrogen concentration (Pd-H sites) is relatively low under CTH conditions. As a consequence, only the SN_1 term (C-OH breaking) is operating. This is a quite rational route especially if we consider that the bond breaking energy of the primary C-OH group in the starting glycerol (79.6 kcal/mol) is strictly comparable with that of benzyl alcohol (~ 80 kcal/mol) and relatively much lower than that calculated for the analogous ethanol (93.5 kcal/mol) so that the OH interaction with the catalyst surface is able to facilitate the C-OH bond breaking [31].

The involvement of hydroxyacetone in transfer hydrogenolysis reactions has raised numerous queries about its role in the overall mechanism. It was shown [3c] that a competitive adsorption between glycerol and AC can occur on the catalyst surface, preventing AC to undergo hydrogenation reaction to

1,2-PDO. With the aim to clarify if hydroxyacetone is an intermediate in the CTH of glycerol, the hydrogenation of AC with 2-propanol as H-source was also studied (Table 5).

In reference experiments, the AC transfer hydrogenation was tested over pure Co_3O_4, CoO, Fe_3O_4, Fe_2O_3 and SiO_2: the reaction did not provide any conversion of AC to 1,2-PDO, confirming that the presence of Pd is essential for the hydrogenation reaction of AC.

In presence of Pd-based catalysts and under CTH conditions, AC conversion decreases in the order Pd/Co > Pd/Fe > Pd/Fe_3O_4 > Pd/Fe_2O_3 ≅ Pd/Co_3O_4 > Pd/CoO ≅ Pd/SiO_2 that is parallel to the dehydrogenation ability of 2-propanol evidenced by our catalysts. In the case of coprecipitated catalysts reactions proceed more rapidly. On using the Pd/Co catalyst, AC was fully converted to 1,2-PDO (85,8%) and 1-PO (14,2%) within 8 hours. Similarly, once AC was allowed to react under CTH conditions in presence of the coprecipitated Pd/Fe catalyst, after 4 and 8 hours, 1,2-PDO was obtained as the only reaction product (100% selectivity) with a conversion, respectively, of 48 and 95%. The whole of hydroxyacetone CTH results allows to achieve two important conclusions: (i) AC is definitely a reaction intermediate in the conversion of glycerol to 1,2-PDO in presence of 2-propanol as H-source and (ii) the formation of 1-PO only occurs after the complete conversion of AC into 1,2-PDO.

The proposed mechanism involves, as final step, the transfer hydrogenation of AC to 1,2-PDO. This may occur through the direct transfer of hydrogen from 2-propanol to AC mediated by the catalytic surface (Scheme 1 c-1) or by the transfer of the hydrogen atom from Pd-H species (formed by dehydrogenation of 2-propanol) to the carbonyl double bond, as it normally occurs in classical hydrogenation reactions (Scheme 1 c-2).

The first route, generally accounted in homogeneous phase [32], was recently thoroughly demonstrated to occur also under heterogeneous conditions [33] in the transfer hydrogenation of cellulose-based oligomers.

Scheme 1 about here

5. Conclusions

The catalytic transfer hydrogenolysis (CTH), promoted by supported palladium catalysts was investigated. Coprecipitated palladium catalysts on cobalt oxide and iron oxide supports allow a complete conversion of glycerol to 1,2-PDO and EG under mild reaction conditions by using 2-propanol as hydrogen donor. Analogous impregnated samples as well as the commercial Pd/SiO_2 catalyst were found to be poorly active in CTH reactions. A tight correspondence between the tendency of catalysts to dehydrogenate 2-propanol and the ability to afford CTH reactions was also found.

The physico-chemical characterization of the broad set of Pd catalysts chosen allows us to conclude that the coprecipitation method ensures a strong interaction between palladium and support leading to formation of bimetallic ensambles which positively promote the glycerol CTH reaction.

The catalytic tests clearly evidence that hydroxyacetone (AC) is an intermediate in the CTH of glycerol so that it is possible to conclude that the most convincing mechanism involves the C-OH breaking of the primary alcoholic group promoted by surface Pd-Me (Co or Fe) ensembles leading to AC that is then reduced to 1,2-PDO.

Acknowledgements

The financial support by Catalysis Research Center, Hokkaido University (Overseas Research Fellow 2013) and MIUR (PRIN2010 - 2010KHLKFC_001) are gratefully acknowledged. The authors express thanks to the technical support of the CRC Technical division for the XPS and TEM measurements.

References

[1] [1a] C. O. Tuck, E. Pérez, I. T. Horváth, R. A. Sheldon, M. Poliakoff, Science 337 (2012) 695-699; [1b] P.Gallezot, Chem. Soc. Rev. 41 (2012) 1538-1558.

[2] [2a] A. M. Ruppert, K. Weinberg, R. Palkovits, Angew. Chem. Int. Ed. 51 (2012) 2564-2601; [2b] N. Yan, P. J. Dyson, Curr. Opin. in Chem. Engin. 2 (2013) 178–183; [2c] J. Ten Dam, U Hanefeld ChemSusChem 4 (2011) 1017-1034; [2d] J.P. Ma, W.Q. Yu, M. Wang, X.Q. Jia, F. Lu, J. Xu Chin. J. Catal. 34 (2013) 492-507.

[3] (3a) J. Jae, W. Zheng, R. F. Lobo, D. G. Vlachos, ChemSusChem 6 (2013) 1158-1162;, (3b) A. Martin, U. Armbruster, I. Gandarias, P. L. Arias, Eur. J. Lipid Sci. Technol. 115 (2013) 9–27; (3c) I. Gandarias, P.L. Arias, J. Requies, M. El Doukkali, M.B. Güemez, J. Catal. 282 (2011) 237–247.

[4] (4a) M. Pagliaro, M. Rossi, The Future of Glycerol, second ed., Royal Society of Chemistry, Cambridge, 2010; (4b) Z. Y. Zakaria, N. A. S. Amina, J. Linnekoski, Biomass and Bioenergy 55 (2013) 370-385; (4c) N.H. Tran, G.S.K. Kannangara, Chem. Soc. Rev. 42 (2013) 9454-9479; (4d) C.H. Zhou, H. Zhao, D. S. Tong, L. M. Wu, W. H. Yu, Catalysis Reviews: Science and Engineering, 55 (2013) 369-453.

[5] (5a) C.H. Zhou, J. N. Beltramini, Y.-X. Fan, G. Q. Lu, Chem. Soc. Rev. 37 (2008) 527-549; (5b) Y. Nakagawa, K. Tomishige, Catal. Sci. Technol. 1 (2011), 179-190; (5c) F. Mauriello, M.G. Musolino, R. Pietropaolo in: M. De Santos Silva, P.C. Ferreira (Eds.), Glycerol: Production, Structure and Applications, Nova Science Publishers, Inc. New York, 2012, pp. 45-75.

[6] (6a) Y. Hu, Y.Q. Fan, Y. Pei, M.H. Qiao, K.N. Fan, X.X. Zhang, B.N. Zong, ACS Catal. 3 (2013) 2280–2287; (6b) J. Hu, X. Liu, Y.Q. Fan, S.H. Xie, Y. Pei, M.H. Qiao, K.N. Fan, X.X. Zhang, B.N. Zong, Chin. J. Catal. 34 (2013) 1020–1026; (6c) J. T. Dam, K. Djanashvili, F. Kapteijn, U. Hanefeld, ChemCatChem 5 (2013) 497–505; (6d) J. Hu, X. Liu, B. Wang, Y. Pei, M. H. Qiao, K.N. Fan, Chin. J. Catal., 33 (2012) 1266–1275; (6e); M. Balaraju, K. Jagadeeswaraiah, P. S. Sai Prasad, N. Lingaiah, Catal. Sci. Technol., 2 (2012) 1967-1976; (6f) S. Zhu, Y. Zhu, S. Hao, H. Zheng, T. Mo, Y. Li,

Green Chem. 14 (2012) 2607-2616; (6g) I. Jiménez-Morales, F. Vila, R. Mariscal, A. Jiménez-López Applied Catalysis B: Environmental 117– 118 (2012) 253– 259

[7] J. Liu, B. Sun, J. Hu, Y. Pei, H. Li, M. Qiao, J Catal. 274 (2010) 287-295.

[8] C-T Wu, K. M. K. Yu, F. Liao, N. Young, P. Nellist, A. Dent, A. Kroner, S. C. E. Tsang, Nature Commun. 3 (2012) 1050

[9] M.G. Musolino, C. Busacca, F. Mauriello, R. Pietropaolo, App. Catal. A: General 379 (2010) 77-86.

[10] (10a) M. G. Musolino, L. A. Scarpino, F. Mauriello, R. Pietropaolo, ChemSusChem 4 (2011) 1143-1150; (10b) J. Ge, Z. Zeng, F. Liao, W. Zheng, X. Hong, S. C. E. Tsang Green Chem., 15 (2013) 2064-2069.

[11] M. G. Musolino, L. A. Scarpino, F. Mauriello, R. Pietropaolo, Green Chem. 11 (2009) 1511-1513.

[12] D. Scholz, C. Aellig, I. Hermans, ChemSusChem 7 (2014) 268-275

[13] F. Schüth, M. Hesse, K. K. Unger, Handbook of Heterogeneous Catalysis, Wiley-VCH Verlag GmbH & Co. KGaA, 2008.

[14] International Center for Diffraction Data, Powder Diffraction Database, Pennsylvania, PA, 1997.

[15] M. Vondrova, T. Klimczuk, V. L. Miller, B. W. Kirby, N. Yao, R. J. Cava, A.B. Bocarsly, Chem. Mater. 17 (2005) 6216-6218.

[16] L.S.F. Feio, C.E. Hori, L.V. Mattos, D. Zanchet, F.B. Noronha, J.M.C. Bueno, App. Catal. A: General 348 (2008) 183-192.

[17] M. L. Toebes, J. A. Van Dillen, K. P. De Jong, J. Mol. Catal. A: Chemical 173 (2001) 75–98

[18] (18a) B.A. Sexton, A.E. Hughes, T.W. Turney, J. Catal. 97 (1986), 390-406; (18b) Y. Ji, Z. Zhao, A. Duan, G. Jiang, Jian Liu, J. Phys. Chem. C 113 (2009) 7186-7199; (18c) H. Zhou, J. Song, H. Fan, B. Zhang, Y. Yang, J. Hu, Q. Zhua, B. Han, Green Chem. 16 (2014) 3870-3875.

[19] J. Zielinski, I. Zglinicka, L. Znak, Z. Kaszkur, Appl. Catal., A: Gen. 381 (2010) 191-196.

[20] H. Y. Lin, Y. W. Chen, C. Li, Thermochim. Acta 400 (2003) 61-67.

[21] F.B. Noronha, M. Schmal, C. Nicot, B. Moraweck, R. Fréty, J. Catal. 168 (1997) 42–50.

[22] A. J. R. Hensley, Y. Hong, R. Zhang, H. Zhang, J. Sun, Y. Wang, J. S. McEwen, ACS Catal. 4 (2014) 3381-3392.

[23] C. D. Wanger, W. M. Riggs, L. E. Davis, J. F. Moulder, G. E.Muilenberg, Handbook of X-ray Photoelectron Spectroscopy, Perkin-Elmer Corp., Minnesota, USA, 1979.

[24] (24a) M. L. Cubeiro, J. L. G. Fierro, J Catal 179 (1998) 150–162; (24b) K. Sun, W. Lu, M. Wang, X. Xu, Appl. Catal. A 268 (2004) 107-113; (24c) A. F. Carlsson, M. Naschitzki, M. Ba1umer, H. J. Freund, J. Phys. Chem. B 107 (2003) 778-785; (24d) M. S. Yalfani, S. Contreras, J. Llorca, M. Dominguez, J. E. Sueirasa, F. Medina, Phys. Chem. Chem. Phys. 12 (2010) 14673-14676; (24e) S. Marx, A. Baiker, J. Phys. Chem. C 113 (2009) 6191-6201.

[25] (25a) F. Mauriello, E. Garrone, M. G. Musolino, R. Pietropaolo, B. Onida, J. Mol. Catal. A: Chemical 328 (2010) 27-34; (25b) F. Mauriello, M. Armandi, B. Bonelli, B. Onida, E. Garrone, J. Phys. Chem. C 114 (2010) 18233-18239

[26] Y. Li, H. Liu, L. Maab, D. He, RSC Adv. 4 (2014) 5503-5512

[27] X. Guo, Y. Li, W. Song, W. Shen, Catal. Lett. 141 (2011) 1458-1463.

[28] B. Li, J. Wang, Y. Yuan, H. Ariga, S. Takakusagi, K. Asakura, ACS Catal. 1 (2011) 1521-1528.

[29] [29a] J. Auneau, C. Michel, F. Delbecq, C. Pinel, P. Sautet, Chem. Eur. Journal 17 (2011) 14288-14299; [29b] D. Coll, F. Delbecq, Y. Arayb, P. Sautet, Phys. Chem. Chem. Phys. 13 (2011) 1448-1456; [29c] B. Liu, J. Greeley, Phys. Chem. Chem. Phys. 15 (2013) 6475-6485; [29d] C. Hadad, C. Callam, S. Singer, T. Lowary, J. Am. Chem. Soc. 123 (2001) 11743-11754.

[30] (30a) N. Thakar, N. F. Polder, K. Djanashvili, H. Van Bekkum, F. Kapteijn, J. A. Moulijn, J. Catal. 246 (2007) 344-350; (30b) M.G. Musolino, F. Mauriello, C. Busacca, R. Pietropaolo, unpublished results.

[31] Y. R. Luo, Comprehensive Handbook of Chemical Bond Energies, CRC Press, Boca Raton, USA, 2007.

[32] S. M. Samec, J. E. Backvall, P. G. Andersson, P. Brandt, Chem. Soc. Rev. 35 (2006) 237-248.

[33] A.Shrotri, H. Kobayashi, A. Tanksale, A. Fukuoka, J. Beltramini, ChemCatChem 6 (2014) 1349-1356.

Graphical Abstract

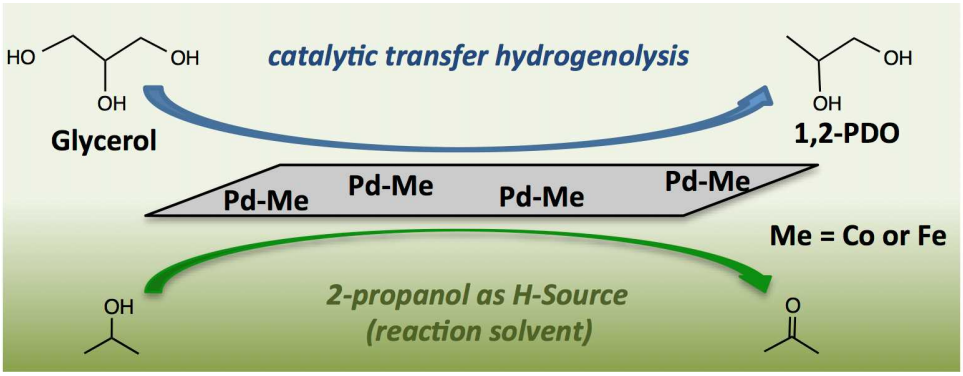

Highlights

- The transfer hydrogenolysis of glycerol is promoted by coprecipitated Pd-catalysts
- The reaction solvent (2-propanol) was used as hydrogen-donor
- Pd-Co and Pd-Fe ensembles have been identified as the active catalytic phases
- CTH mechanism involves the glycerol dehydration and subsequent hydrogenation

Table 1

Main characteristics of the supported palladium catalysts investigated (S.A. = surface area; d_n = Mean particle size from TEM; S_{act} = Active surface area calculated by CO-pulse chemisorption technique based and an assumption of CO/Pd = 1).

Catalyst notation	**Support**	**Catalyst source/preparation**	**Pd loading (wt%)**	**S.A. (m^2/g)**	**S_{act} (m^2/g)**	**d_n (nm)**
Pd/Co	Co_3O_4	co-precipitation	3.7	106	9.70	10.7
Pd/CoO	CoO	impregnation	4.5	8	1.20	4.3
Pd/Co_3O_4	Co_3O_4	impregnation	5.1	70	5.31	7.8
Pd/Fe	Fe_3O_4	co-precipitation	8.7	170	2.51	1.8
Pd/Fe_3O_4	Fe_3O_4	impregnation	5.2	60	0.23	8.8
Pd/Fe_2O_3	Fe_2O_3	impregnation	5.5	6	1.22	7.1
Pd/SiO_2	SiO_2	commercial	5.0	500	0.85	12.2

Table 2

Binding energy values of Pd $3d_{5/2}$, $Co2p_{3/2}$ and O_{1s} levels in Pd/Co, Pd/CoO and Pd/Co_3O_4 catalysts.

Catalysts notation		**Binding Energy (eV)**			
		$Pd3d_{5/2}$	**$Co2p_{3/2}$**	**$Co2p_{3/2}$ sat.**	**O1s**
Pd/Co	*unred*	336.8	779.9	-	531.4
	red	335.2	779.7	785.9	530.4
	in situ red	335.5	778.2	785.9	530.4
Pd/CoO	*unred*	337.1	780.2	786.0	531.4
	red	334.9	780.2	786.0	531.4
	in situ red	334.9	780.2	786.0	531.4
Pd/Co_3O_4	*unred*	337.2	780.1	786.1	531.4
	red	335.0	780.1	786.1	531.4
	in situ red	335.0	780.1	786.1	531.4

Table 3

Binding energy values of Pd $3d_{5/2}$, $Fe2p_{3/2}$, and O_{1s} levels in Pd/Fe, Pd/Fe_3O_4 and Pd/Fe_2O_3 catalysts.

Catalysts notation		**Binding Energy (eV)**			
		$Pd3d_{5/2}$	**Fe2p3/2**	**Fe2p3/2 sat.**	**O1s**
Pd/Fe	*unred*	336.5	710.9	718.5	530.2
	red	335.2	710.7	-	530.2
	in situ red	335.3	710.7	-	530.2
Pd/Fe_3O_4	*unred*	336.5	710.5	-	530.1
	red	334.8	710.5	-	530.1
	in situ red	334.8	710.5	-	530.0
Pd/Fe_2O_3	*unred*	336.6	710.4	718.4	530.0
	red	334.8	710.4	718.5	530.0
	in situ red	334.8	710.4	718.5	530.0

Table 4

Glycerol transfer hydrogenolysis promoted by supported palladium catalysts, carried out at 453 K and 0.5 MPa N_2 pressure for 24 h. 1,2-PDO = 1,2-propanediol; EG = ethylene glycol; 1-PO = 1-propanol; AC = 1-hydroxyacetone; OP = other products

Catalysts notation	**Conversion (%)**	**Selectivity (%)**				
		1,2-PDO	**EG**	**1-PO**	**AC**	**OP**
Pd/Co	100	64.0	8.2	24.9	-	2.9
Pd/Co_3O_4	37,9	14.6	6.1	-	37.4	41.9
Pd/CoO	2.9	-	-	-	100	-
Pd/Fe	100	55.9	1.8	-	25.2	17.0
Pd/Fe_3O_4	66.5	47.7	8.0	-	44.3	0
Pd/Fe_2O_3	40.4	26,6	6.6	-	58.1	8.7
$PdSiO_2$	0.5	-	-	-	100	-

Table 5

Hydroxyacetone transfer hydrogenolysis promoted by supported palladium catalysts, carried out at 453 K and 0.5 MPa N_2 pressure. 1,2-PDO = 1,2-propanediol; 1-PO = 1-propanol; OGP = other gas-phase products

Catalysts notation	**Reaction Time (h)**	**Conversion (%)**	**Selectivity (%)**	
			1,2-PDO	**1-PO**
Pd/Co	8	100	85,8	14,2
Pd/Co	4	65,1	100	-
Pd/Co_3O_4	24	25,5	100	-
Pd/CoO	24	12,1	100	-
Pd/Fe	8	95,1	100	-
Pd/Fe	4	48,5	100	-
Pd/Fe_3O_4	24	55,2	100	-
Pd/Fe_2O_3	24	30,0	100	-
$PdSiO_2$	24	9,8	100	-

Figure captions

Fig. 1. XRD patterns of the investigated palladium catalysts.

Fig. 2. TEM images of Pd/Co, Pd/CoO and $PdCo_3O_4$ catalysts at 50 and 5 nm and relative particles size distribution.

Fig. 3. TEM images of Pd/Fe, Pd/Fe_3O_4 and $PdFe_2O_3$ catalysts at 50 and 5 nm and relative particles size distribution.

Fig. 4. H_2-TPR profiles of the investigated palladium catalysts.

Fig. 5. XPS Co $2p_{3/2}$ and Fe $2p_{3/2}$ plots in Pd/Co and Pd/Fe catalysts: unreduced (a), reduced (b) and in situ reduced (c).

Fig. 6. XPS Pd $2p_{3/2}$ plots of coprecipitated and impregnated catalysts.

Fig. 7. Acetone formation (mol/l) and conversion of glycerol (%) in CTH reaction promoted by supported Pd-catalysts.

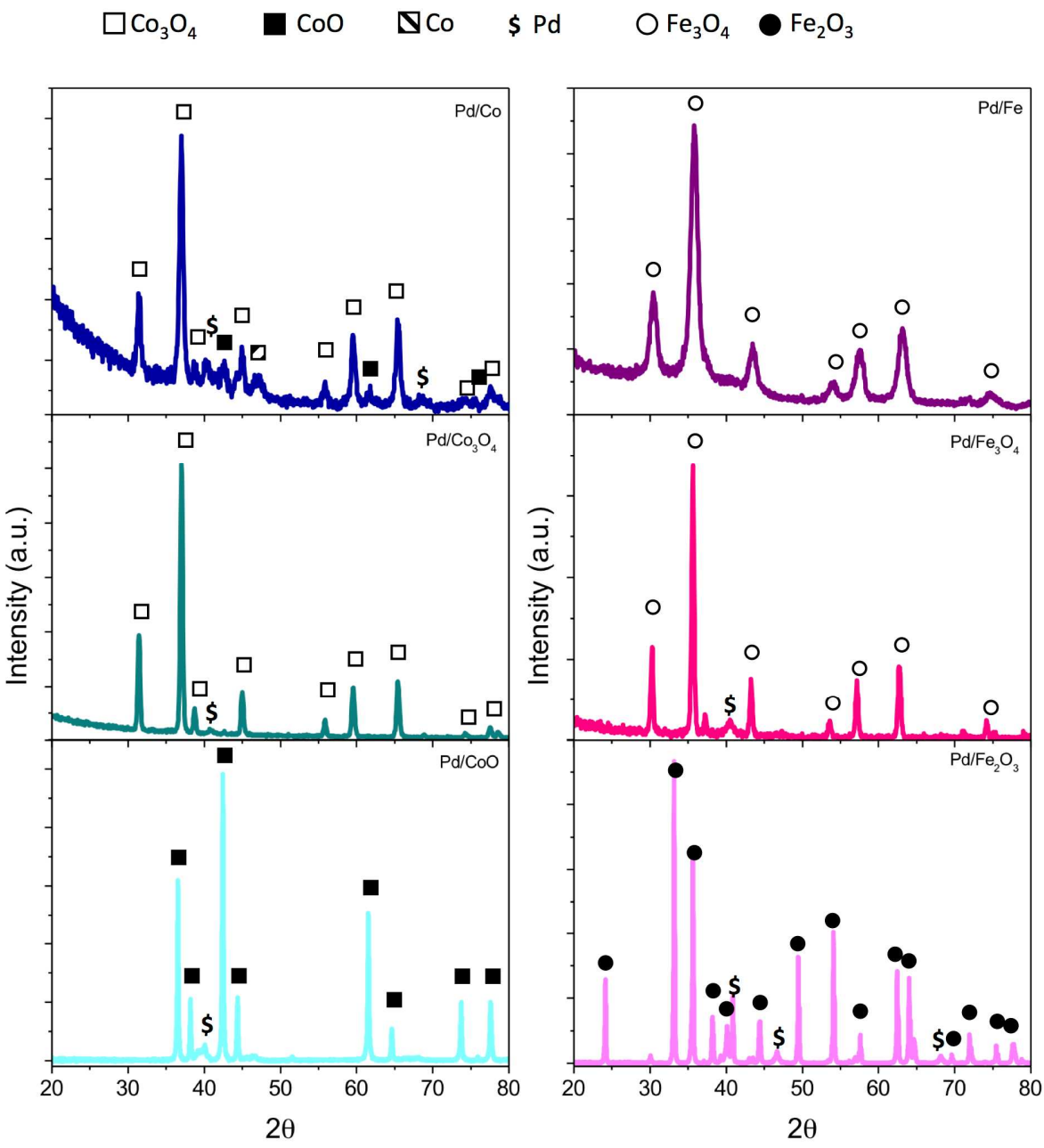

Fig. 1. XRD patterns of the investigated palladium catalysts.

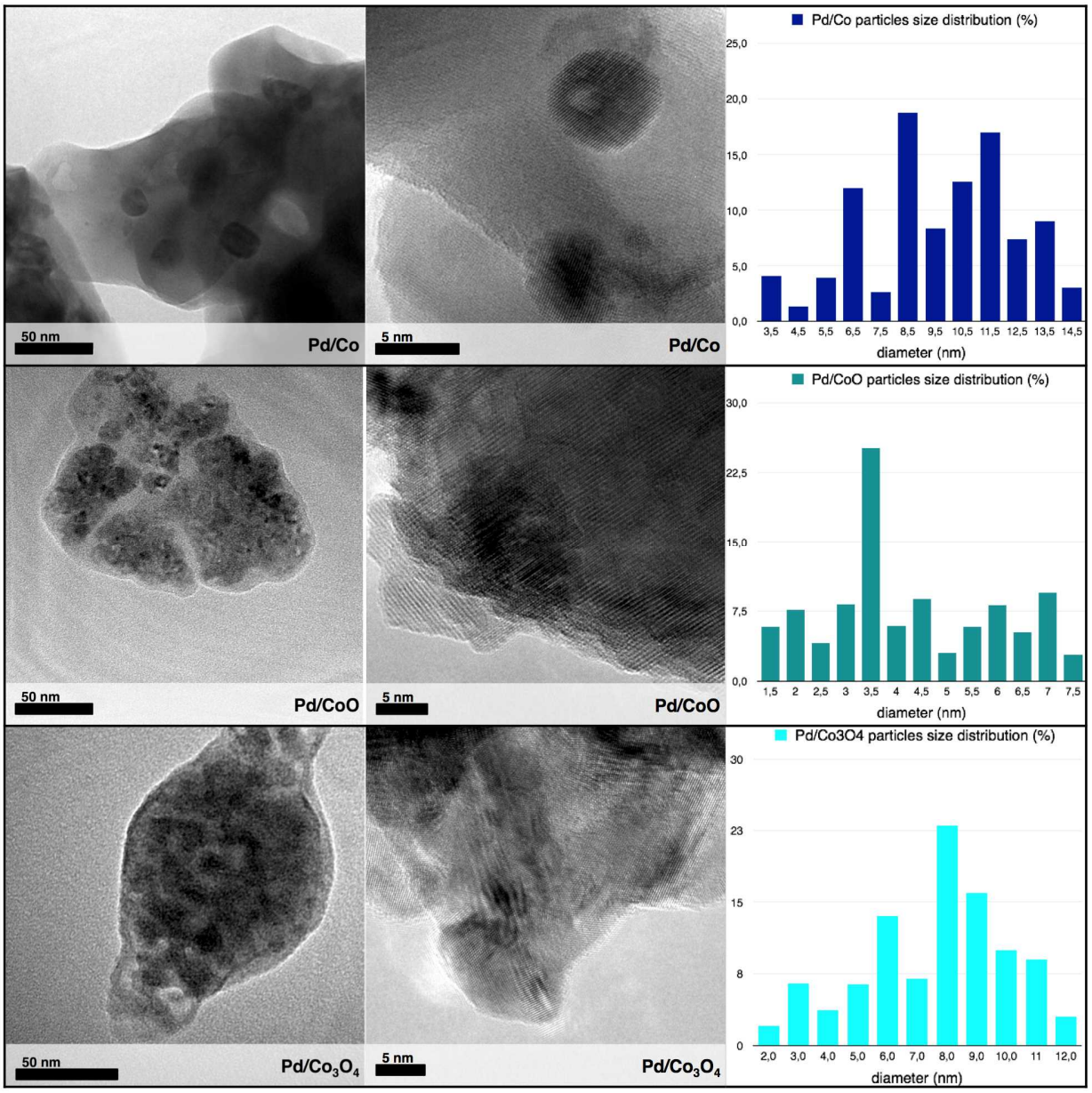

Fig. 2. TEM images of Pd/Co, Pd/CoO and $PdCo_3O_4$ catalysts at 50 and 5 nm and relative particles size distribution.

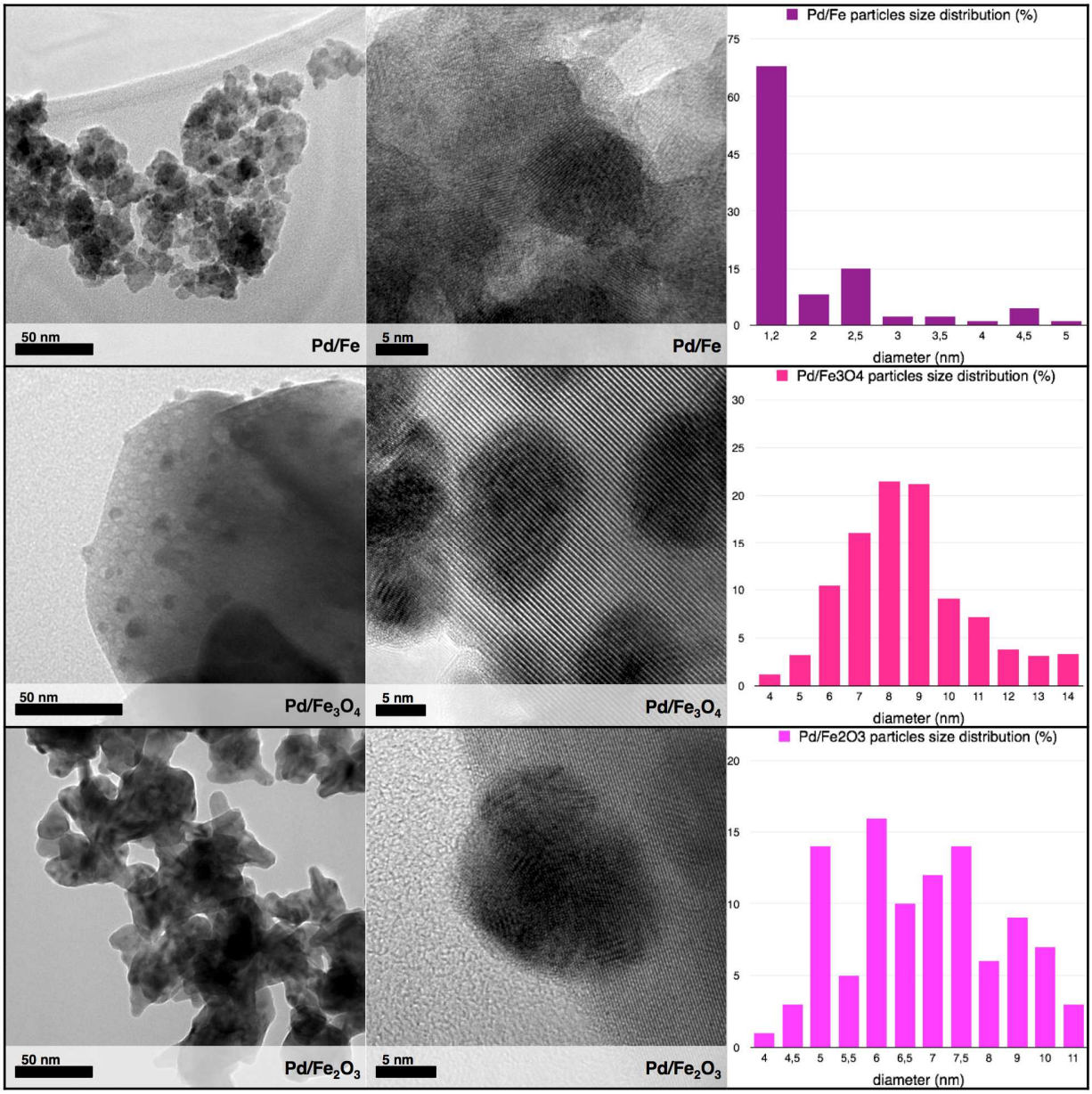

Fig. 3. TEM images of coprecipitated and impregnated palladium catalysts.

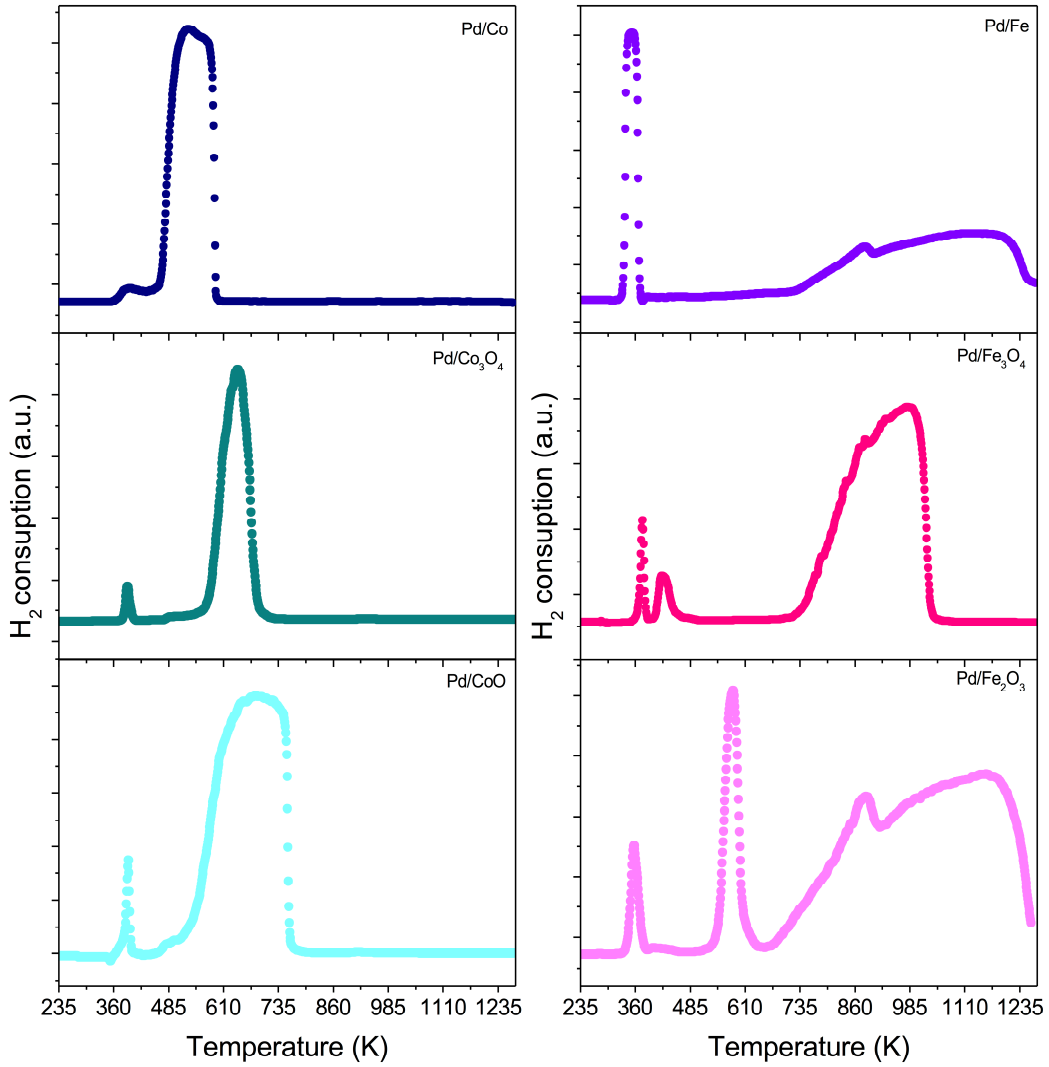

Fig. 4. H_2-TPR profiles of the investigated palladium catalysts.

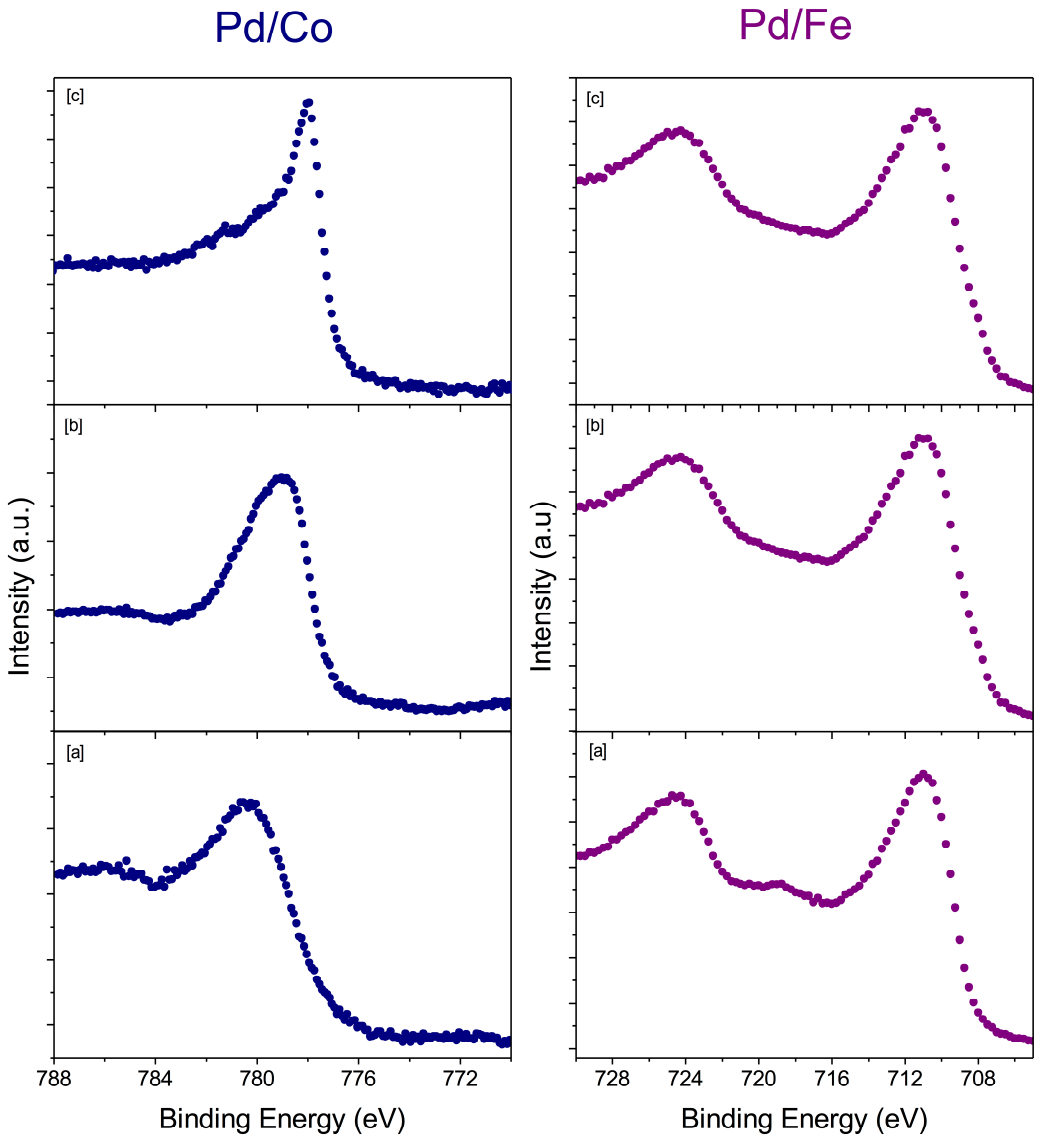

Fig. 5. XPS Co $2p_{3/2}$ and Fe $2p_{3/2}$ plots in Pd/Co and Pd/Fe catalysts: unreduced (a), reduced (b) and in situ reduced (c).

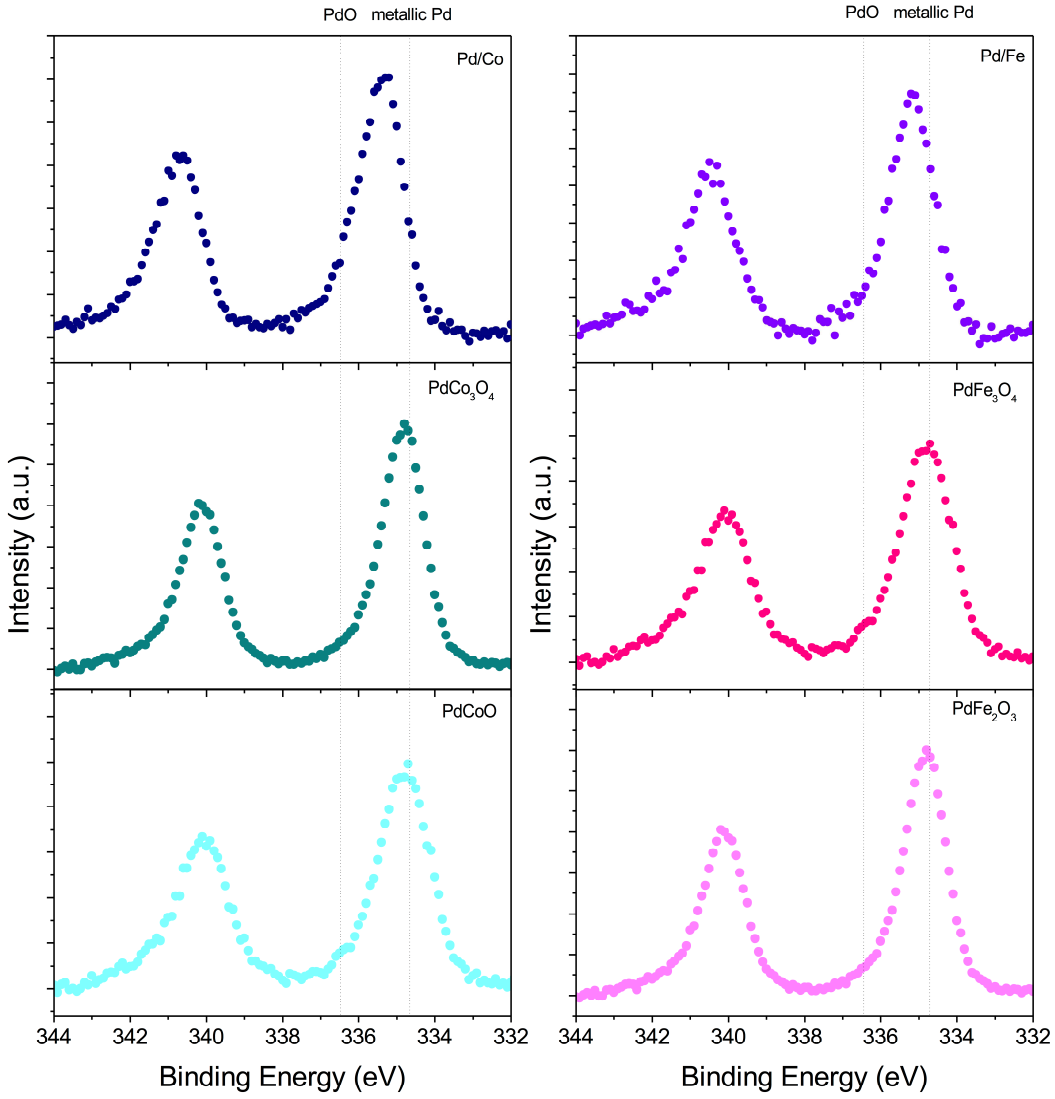

Fig. 6. XPS Pd $2p_{3/2}$ plots of coprecipitated and impregnated catalysts.

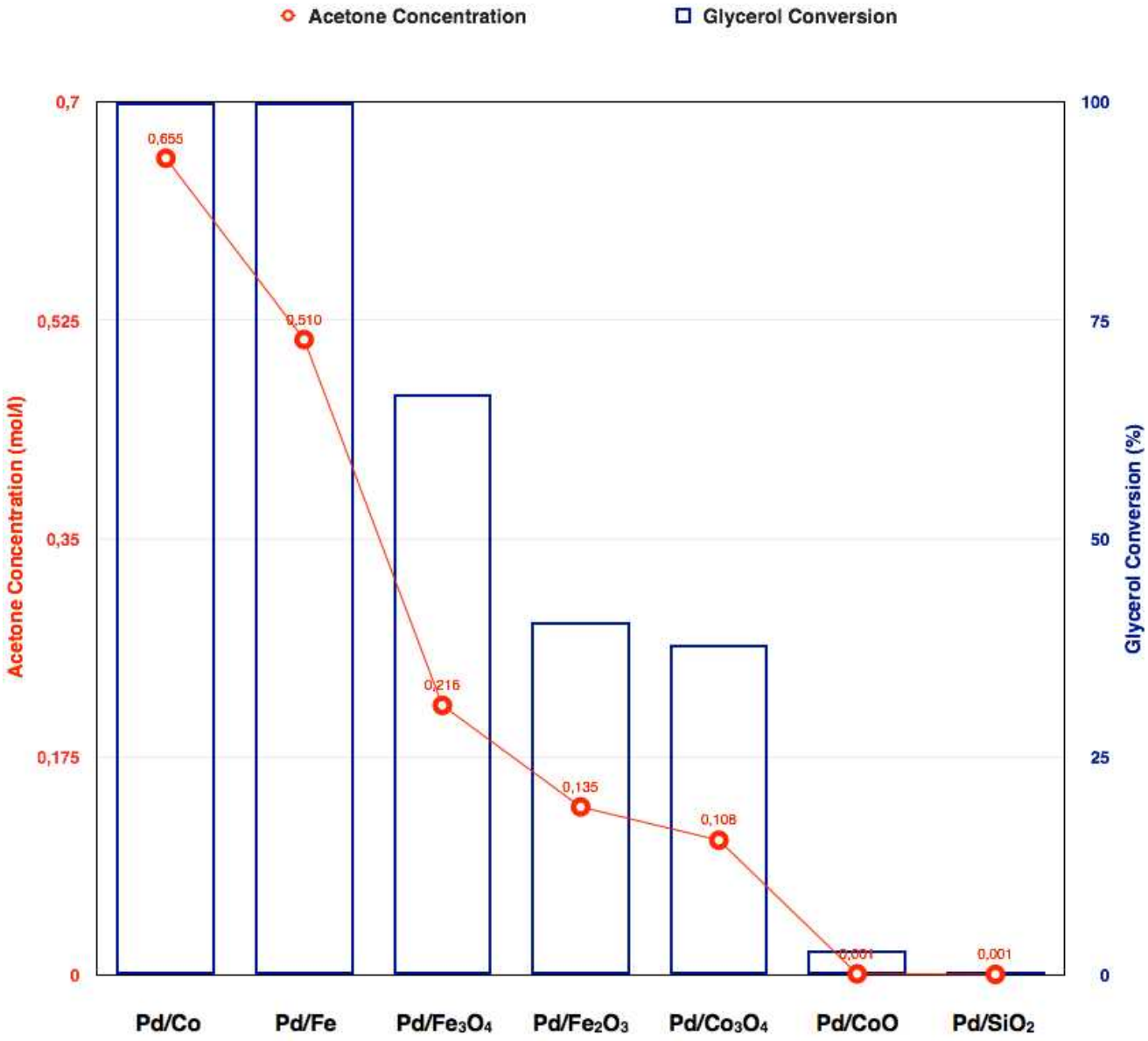

Fig. 7. Acetone formation (mol/l) and conversion of glycerol (%) in CTH reaction promoted by supported Pd-catalysts.

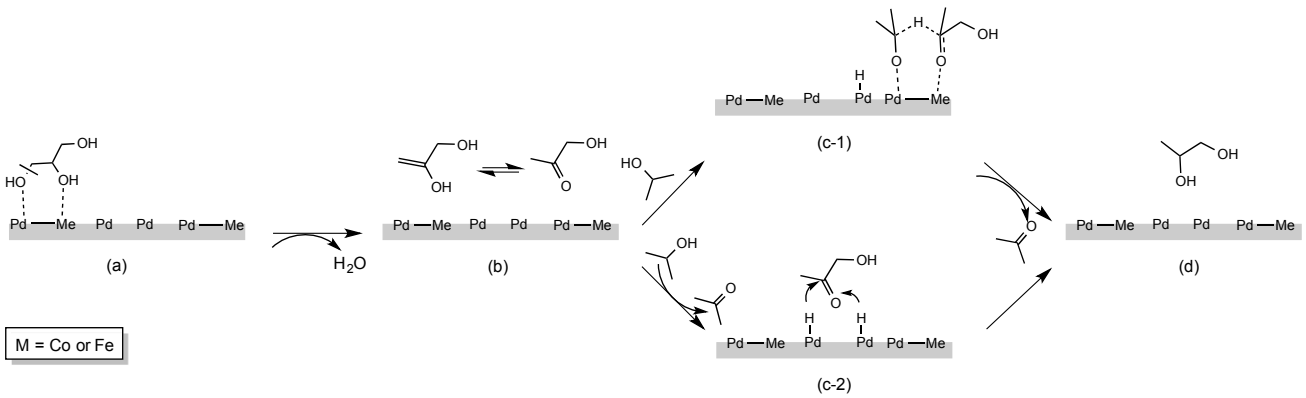

Scheme 1